WARWICK
THE UNIVERSITY OF WARWICK

Manuscript version: Author's Accepted Manuscript
The version presented in WRAP is the author's accepted manuscript and may differ from the published version or Version of Record.

Persistent WRAP URL:
http://wrap.warwick.ac.uk/168367

How to cite:
Please refer to published version for the most recent bibliographic citation information. If a published version is known of, the repository item page linked to above, will contain details on accessing it.

Copyright and reuse:
The Warwick Research Archive Portal (WRAP) makes this work by researchers of the University of Warwick available open access under the following conditions.

Copyright © and all moral rights to the version of the paper presented here belong to the individual author(s) and/or other copyright owners. To the extent reasonable and practicable the material made available in WRAP has been checked for eligibility before being made available.

Copies of full items can be used for personal research or study, educational, or not-for-profit purposes without prior permission or charge. Provided that the authors, title and full bibliographic details are credited, a hyperlink and/or URL is given for the original metadata page and the content is not changed in any way.

Publisher's statement:
Please refer to the repository item page, publisher's statement section, for further information.

For more information, please contact the WRAP Team at: wrap@warwick.ac.uk.

warwick.ac.uk/lib-publications

Contact Force Sensing and Control for Inserting Operation During Precise Assembly Using a Micromanipulator Integrated with Force Sensors

Beichao Shi, Fujun Wang, Zhichen Huo, Yanling Tian, Ren Cong, Dawei Zhang

***Abstract*—This paper proposes a novel contact force sensing and control method for the inserting operation during precise assembly process, which is based on a micromanipulator integrated with force sensors. At first, theoretical analysis is carried out to calculate the admissible contact force between the gripped holes and the pegs. The contact force thresholds which are smaller than the admissible contact forces are adopted in the control algorithm to avoid the rotating of the gripped holes during assembly process. The force sensors are calibrated using an ATI force sensor and the conversing coefficients are calculated. The admissible contact forces are tested when different contact distance and preload force are adopted. The performance of the proposed contact force sensing and control method is verified by carrying out the task of applying contact force on the surface of the gripped holes with different contacting speeds. The results indicate that the contact force can be adjusted to be smaller than the threshold 1 and the peg-in-hole assembly can be completed successfully.**

***Note to Practitioners*—This paper proposes a novel contact force sensing method during the inserting operation. Compared with the traditional contact force sensing method, this paper adopts the force sensor integrated into the micromanipulator instead of commercial force sensor to detect the contact force between two parts. To ensure the assembling precision, the theoretical analysis is conducted to calculated the admissible contact force to avoid the sliding and rotating of the gripped micro part during assembling. This work efficiently simplifies the contact force sensing and control process, where complex calibration process needn't to be carried out to eliminate the influence of the mass of the micromanipulator on the testing results. In addition, the assembling costs are reduced by replacing commercial force sensors with strain gauges.**

***Index Terms*—Admissible contact force, integrated force sensor, micromanipulator, contact force controller, precise assembly**

I. Introduction

With the rapid development of micro devices and micro systems, precise assembly technology is becoming more and more important to produce complex micro devices constructed with different micro parts [1-4]. As a representative assembly operation, precise peg-in-hole assembly has attracted wide attention from researchers [5-7].

The micro parts manipulated in precise assembly process are usually designed with the size ranging from several micrometers to millimeters which requires micron-level assembly precision [8, 9]. Generally, precise robot is needed to be designed to complete this task [10-12]. Microscopic vision is usually used to guide the motion of the micro assembly robot and achieve precise alignment during micro assembling process. However, the inherent characteristics of visual servo of small view field and inability to detect assembly stress limits the manipulation ability [13, 14]. In addition, the relative position and pose between the micro parts to be assembled cannot be distinguished by micro vision system when occlusion occurs. To overcome this problem, the contact forces between the micro parts are introduced to reflect the relative position during precise assembly. In order to improve the assembly precision, researchers have proposed several methods to detect and control the contact forces.

Due to the occlusion during assembling process, a contact force controller was adopted to detect the relative position between the manipulator and the operated ring to achieve precise alignment [13]. A conversion coefficient was introduced to determine whether the force controller is required. However, the controlling precision is related to the conversion coefficient which is determined by operator's experience. Automated and intelligent assembly process was achieved by mapping the relationship between the contact force and position [15]. The performance of the assembly method was verified by inserting a peg into a hole automatically. Technically, enormous experimental tests and intelligent algorithm are needed to establish the relationship between position and force which makes the control process complex. Liu et al. proposed an automatic precise assembly system where three microscopes were used to align the two micro parts and the force sensor was used to detect the contact states during inserting process [16]. An efficient assembling strategy based on contact force controller was developed in Ref. [17], where the partially

This research is supported by National Key R&D Program of China (no. 2019YFB1310902), National Natural Science Foundation of China (Grant no. 51675376).

B. Shi, F. Wang, Z. Huo, R. Cong and D. Zhang are with Key Laboratory of Mechanism Theory and Equipment Design of Ministry of Education, School of Mechanical Engineering, Tianjin University, Tianjin 300354, China (e-mail: shi0802@tju.edu.cn; wangfujun@tju.edu.cn; huozhichen@tju.edu.cn; 3017201184@tju.edu.cn; medzhang@tju.edu.cn). (Corresponding author: Fujun Wang).

Y. Tian is with School of Engineering, University of Warwick, Coventry CV4 7AL, UK (y.tian.1@warwick.ac.uk).

flexible peg can be inserted into the hole precisely. Hou et al. proposed a peg-in-hole assembly method based on fuzzy logic-driven variable time-scale prediction-based reinforcement learning, where the assembly dual pegs and holes was completed [18]. All the above work can complete precise assembly of micro parts based on the commercial force sensor. However, the force threshold used in the contact force controller is adopted according to experience. The conversion is required between the force collected by the sensor and the force applied on the micro parts. In addition, complex calibration process is required to be carried out to eliminate the influence of the mass of the micromanipulator on the testing results.

Generally, micromanipulators, such as piezoelectric micromanipulators [19-21], electrostatic micromanipulators [22, 23], vacuum adsorbers [24] are used to manipulate micro parts directly. Usually, the force sensors are integrated into the micromanipulator to monitor the grasping force to avoid damaging the micro parts. In order to simplify the micro assembly system, these integrated force sensors can also be used to detect the contact forces between the micro parts and the environment. Bilal et al. [25] used two commercial force sensors where each force sensor comprises a probe to pick and assemble the micro part. Due to the motion of two probes along main direction of the force sensor, the contact force can be easily detected by the force sensors. Compared with the methods mentioned above, the force transmission error can be reduced using this strategy. However, the micro part could rotate or slide during operating process because the admissible lateral contact force was set as a larger value, which could influence the assembling precision. In addition, the grasping force adjusting motion and the motion of the corresponding finger are driven by the same 3-DOF micropositioning stage which makes the contact force control system complex.

To solve these problems, this paper proposes a novel contact force sensing and control method based on a micromanipulator integrated with force sensors. The grasping force between the fingers and micro part, and the contact force between two micro parts are observed by the integrated force sensors. Then, these forces information are used to detect the relative position between the two micro parts to achieve automatic assembly. This paper is organized as follows: the grasping stability analysis is carried out in Section II; Section III describes the inserting control strategy; The experimental tests are conducted to evaluate the performance of the control strategy in Section IV; Finally, Section V concludes this paper.

II. Admissible Contact Force Analysis

An improved micromanipulator which can achieve different grasping modes is developed according to our previous work [26]. Each finger is actuated by one piezoelectric ceramic and the micro parts with different shapes can be grasped by designing different fingers. A flexible beam was designed at one end of these fingers which can be used to estimate the grasping force and lateral contact force by sticking strain gauges on the surface. The micromanipulator integrated with force sensor is installed on a macro-micro precise assembling robot to pick up, transmit and manipulate the micro parts. Combined with another 3-DOF precise positioning stage and visual system, the micro assembly system is established. In this paper, the assembling process of the insertion of cylindrical peg-hole and cuboid peg-hole is studied using this precise assembly system, during which the contact force is used to detected the relative position of the hole and peg.

It's well known that the grasping state will be changed when an external contact force applied on the gripped micro part. To avoid the rotating and sliding of the gripped micro part, the contact force needs to be limited to an appropriate range to keep the balance. Hence, the objective of this section is to establish the mathematical model between the grasping forces, the parameters of the micromanipulator and the grasping state to investigate the behavior of the gripped hole subjected to different contact forces.

A. Stability Analysis During Cuboid Peg-in-Hole Assembling

As shown in Fig. 1, four fingers with planar surface are used to grasp the cuboid hole. To pick the cuboid hole up successfully, preload forces with the amplitude of F_{ri0} (i=1, 2, 3, 4) (where $F_{r10} = F_{r20} = F_{r30} = F_{r40} = F_{r0}$) are applied on the cuboid hole which should fulfil the requirement of $4\mu F_{ri0} \geq mg$. Because there is no contact force applying on the cuboid hole, the action points of the grasping forces are located at the center of the finger-hole interface and there is no relative sliding and rotating between the fingers and the cuboid hole, as shown in Fig. 1(a).

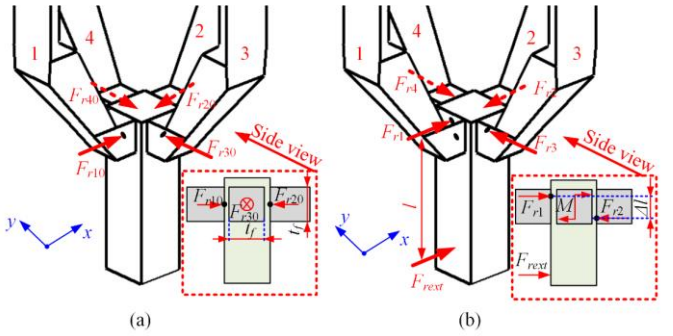

Fig. 1. Cuboid hole gripped by four planar fingers, (a) without contact force, (b) subject to contact force.

During inserting process, the relative position between the peg and the hole cannot be detected by the microscopes and the peg may contact with the inner wall of the hole. The admissible contact force needs to be investigated to prevent the rotating or sliding of the gripped cuboid hole and guarantee the assembling precision. A theoretical model when the gripped cuboid hole is subjected to a contact force along x-axis is established in this paper. Due to the symmetric characteristics, the same method can be used for analysis when the gripped cuboid hole is subjected to a lateral contact force along y-axis.

Firstly, resistant moment generated by finger 3 and finger 4 are calculated. The grasping force can be regarded as the uniform load acting on the interface. The elementary friction force at the unit area can be expressed as

$$df_r = \mu P_{ri} ds \tag{1}$$

where P_{ri} (i= 3, 4) is the unit load, ds is the elementary area and μ is the friction coefficient of the interface.

Then the elementary resistant moment generated by the unit friction force can be evaluated as

$$dT = l\mu P_{ri} ds \tag{2}$$

where l is the distance between the axis of P_{ri} and external force.

To simplify the analysis process, the finger-hole interface is equivalent as a circle with a radius of R, which has the same area as the actual contact surface.

$$R = \sqrt{\frac{t_f^2}{\pi}} \tag{3}$$

where t_f is the thickness of the finger.

Hence, the resistant moment T_{r1} generated by finger 3 and finger 4 can be calculated as

$$T_{r1} = \int_0^R \int_0^{2\pi} l\mu\left(P_{r3} + P_{r4}\right) l d\varphi dl = \frac{4\mu R}{3} F_{r0} \tag{4}$$

In addition, with the increasing of the contact force, the axis of F_{r1} and F_{r2} will move from center to the edge of the interface step by step, as shown in Fig. 2. Due to the bias Δl between the axis of two forces and the interface's center, a resistant moment T_{r2} is generated and can be calculated as

$$T_{r2} = \frac{\Delta l}{2}\left(F_{r1} + F_{r2}\right) \tag{5}$$

The grasping forces $F_{r1}$and F_{r2} can be expressed by F_{ri0} as

$$\begin{aligned} F_{r1} &= F_{r0} - \frac{F_{rext}}{2} \\ F_{r2} &= F_{r0} + \frac{F_{rext}}{2} \end{aligned} \tag{6}$$

When the axis of the grasping force moves to the edge of the contact surface, the largest resistant moment generated by finger 1 and finger 2 can be expressed as

$$T_{r2} = F_{r0} t_f \tag{7}$$

As mentioned above, the total resistant moment T_r induced by four grasping forces can be calculated as

$$T_r = 2T_{r1} + T_{r2} \tag{8}$$

Then, in order to prevent the rotating and sliding of the gripped cuboid hole, the admissible lateral contact force can be evaluated as

$$F_{rext} \le \frac{4\mu F_{r0} R + 3F_{r0} t_f}{3L_r} \tag{9}$$

where L_r is the distance between the axis of F_{rext} and the center of contact surface.

The friction coefficient of aluminum-aluminum interface is selected as 0.3. The thickness of the finger is designed as 2 mm and the equivalent radius R can be calculated as 1.13mm. According to Eq. (9), the relationship among F_{rext}, F_{r0} and L_r can be summarized as shown in Fig. 2. When the cuboid hole is grasped, the admissible lateral contact force is increased with the increasement of preload force, while that is decreased with the increasement of the distance between the center of the interface and the axis of the contact interface. As can be seen from Fig. 2, the maximum admissible lateral contact force is 24.51 mN and 16.35 mN when the preload forces are set as 40 mN and the contact distance is 4 mm and 6 mm, respectively. In order to achieve a stable gripping and guarantee the assembling precision, the combination of preload force and contact distance must be located below the plane shown in Fig. 2.

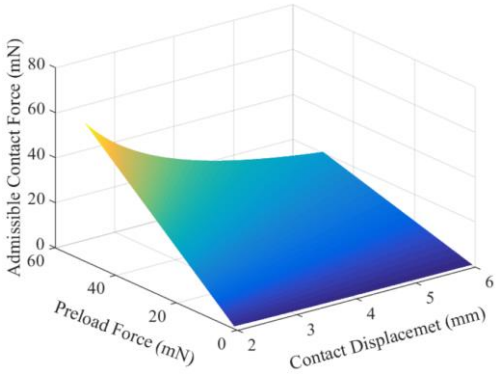

Fig. 2. The relationship between admissible contact force, preload force and the distance in cuboid peg-in-hole assembly.

B. Stability Analysis During Cylindrical Peg-in-Hole Assembling

To achieve stable manipulation, four fingers with arc surface are adopted to grasp the cylindrical hole. Initially, four preload forces F_{ci0} (i=1, 2, 3, 4) (where F_{c10} = F_{c20} = F_{c30} = F_{c40} = F_{c0}) are applied on the cylindrical hole to pick it up. And perfect surface contact can be achieved if there is no contact force applied on the cylindrical hole, as shown in Fig. 3(a). Then, theoretical analysis is carried out to investigate the admissible contact force to maintain stable grasping, during which a lateral contact force along x-axis is applied on the gripped cylindrical hole as shown in Fig. 3(b).

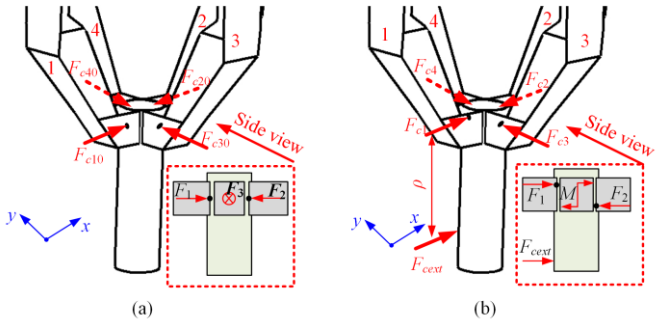

Fig. 3. Cylindrical hole gripped by four planar fingers, (a) without contact force, (b) subject to contact force.

The friction force df_c applied on the unit contact surface can be written as

$$df_c = \mu P_{ci} ds \tag{10}$$

where P_{ci} (i= 3, 4) is the unit pressure. And the friction force is along the tangential direction of the arc surface. As illustrated in Fig. 4, the component dF_{ci} paralleling with x-axis can be derived as

$$dF_{c_i} = \mu P_{ci} ds \cos\varphi \tag{11}$$

where φ is the angle between the axis of P_{ci} and the edge of the arc contact surface, as shown in Fig. 4.

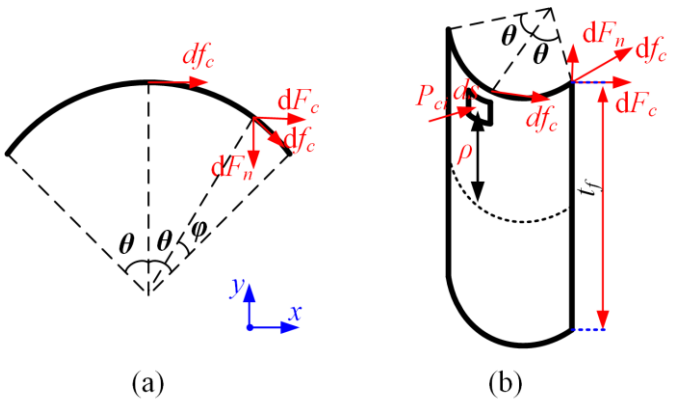

Fig. 4. Detail scheme used to calculate the resistant moment generated by finger 3 and finger 4 in cylindrical peg-in-hole assembly.

Then the resistant moment d_{Tc1} introduced by dF_{ci} can be calculated as

$$dT_{c1} = \rho \bullet dF_{ci} \tag{12}$$

where ρ is the distance between the axis of dF_{ci} and the interface's center. Then the resistant moment T_{c1} generated by friction forces applied by finger 3 and finger 4 can be obtained by integrating dT_{c1} on the arc interface.

$$T_{c1} = 4\int_0^{\frac{t_f}{2}}\int_0^{\theta} \rho\mu\left(P_{c3}+P_{c4}\right)R_c d\varphi d\rho = \frac{\mu F_{c0} t_f \sin\theta}{2\theta} \tag{13}$$

where R_c is the radius of the arc interface, and θ is a half of the central angle corresponding to the arc contact surface.

The other resistant moment generated by finger 1 and finger 2 can be expressed as

$$T_{c2} = F_{c0} t_f \tag{14}$$

Different with the fingers with planar surface, a resistance moment T_{c3} can be exerted on the object by the arc edge of finger 3 and finger 4 when subjected to a contact force.

$$T_{c3} = 2F_{ci} t_f \Delta \tag{15}$$

where Δ is an adjusting coefficient which can be expressed as

$$\Delta = \frac{1-\cos\theta}{2}$$

In summary, when the cylindrical hole is gripped by the arc shape fingers, the total resistant moment generated by four fingers can be evaluated as

$$T_c = T_{c1} + T_{c2} + T_{c3} = F_{ci} t_f \left(\frac{\mu\sin\theta}{2\theta} + 2 - \cos\theta\right) \tag{16}$$

To prevent the rotating and sliding of the cylindrical hole, the admissible lateral contact force should fulfil the following equation

$$F_{cext} \le \frac{F_{c0} t_f}{L_c}\left(\frac{\mu\sin\theta}{2\theta} + 2 - \cos\theta\right) \tag{17}$$

According to the developed micromanipulator, the central angle corresponding to the arc surface of the finger is 80°. The relationship among F_{cext}, F_{c0} and L_c can be plotted as shown in Fig. 5 according to Eq. (17). The admissible contact force is 38.64 mN and 25.76 mN when the preload forces are set as 40 mN and the contact distance is 4 mm and 6 mm, respectively. As can be seen from Fig. 5, in order to prevent rotating and sliding of the cylindrical hole, the contact force should not exceed the admissible lateral contact force corresponding to the contact distance.

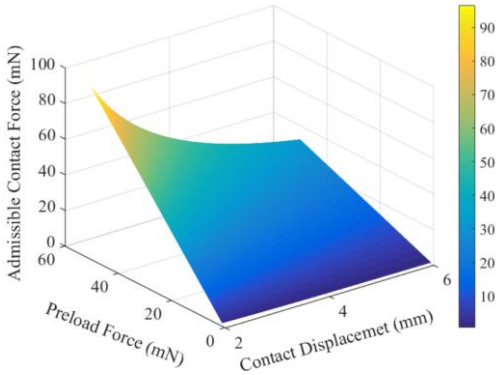

Fig. 5. The relationship between admissible contact force, preload force and the distance in cylindrical peg-in-hole assembly.

III. Contact Force Control Strategy

In order to prevent damaging the peg and hole and achieve precise assembly, a force controller is established where the lateral contact force is adopted to detect the relative position between the peg and hole.

At first, the relative position between the peg and hole is detected and adjusted by visual servo and the position controller is used to achieve precise alignment before assembly. After that, the z-axis platform starts moving forward and the peg starts inserting into the hole. At the same time, the incremental force controller starts working and the lateral contact forces F_x, F_y are collected by the force sensor integrated in the micromanipulator. According to the developed incremental force controller, the peg-in-hole assembling manipulation can be divided into the following three states:

1) If the contact forces F_x and F_y are both smaller than the force threshold 1 (8 mN) which is slightly bigger than the amplitude of noise, the incremental force controller switches off and the peg is inserted into the hole continuously by the forward motion of z-axis platform.
2) If the contact forces F_x or F_y exceeds the force threshold 1 (8 mN) but are less than force threshold 2 which is slightly smaller than the amplitude of admissible contact force, the incremental force controller switches on. The corresponding x-axis or y-axis platform will move step by step to adjust the contact force to be smaller than force threshold 1 and the moving direction of the incremental step is determined by the sign of F_x or F_y. During this step, the inserting operation won't be stopped.
3) When the lateral contact force F_x or F_y exceeds the force threshold 2, the inserting motion stops and the corresponding adjusting platform starts working. The peg will be restarted to insert into the hole when the contact forces are reduced to fulfill the condition of state 2.

The force threshold 2 for different operating conditions can be determined based on the results of the theoretical analysis. It's vital important that the speed of the adjusting motion generated by x-axis platform and y-axis platform should be larger than that of the inserting motion along z-axis to avoid excessive contact force.

IV. Experimental Tests

The experimental setup is displayed in Fig. 6. The macro-micro precise assembling robot with 9-DOF (degree of freedom) was adopted to achieve precise positioning. A 3-DOF translational platform was used to provide the perturbation during validation of the proposed method. The spatial micromanipulator actuated by PZTs (PSt150/5×5×20 L from COREMORROW, Inc.) was installed on the end of the robot. Strain gauges were glued on the surface of the flexible mechanism of the jaw to measure the grasping force and lateral contact force. A dynamic strain gauge system was employed to collect the output signal of the strain gauge. ATI-nano 17 force sensor was used to calibrate the strain gauges and calculate the conversion coefficients between the output voltages and forces. Laser displacement sensor (LK-H050 from Keyence, Inc.) was used to measure the adjusting displacement and inserting displacement, respectively. The signals were collected by a data acquisition board (NI USB-6356).

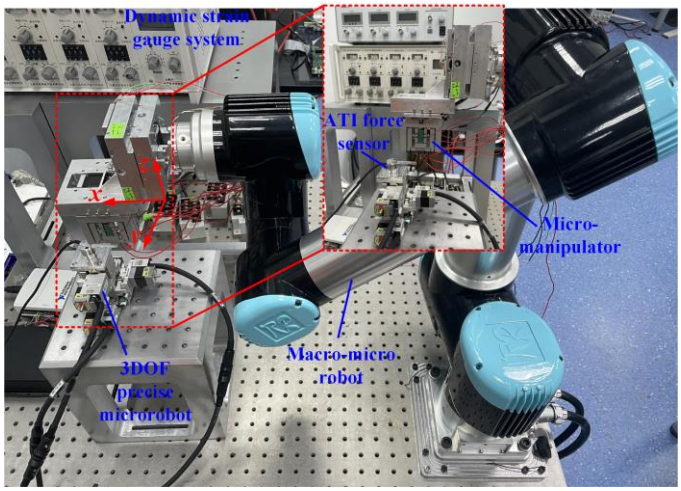

Fig. 6. The experimental setup

Firstly, the relationship between the output voltages of strain gauges glued on four fingers and the grasping forces were calibrated. A precise force sensor ATI nano-17 was selected to apply series of forces on the four fingers, respectively. Then, the known forces and the corresponding voltages signals were collected. According to the test results, the conversion coefficients between the output voltage signal of each strain gauge glued on fingers with arc surface and the known force can be obtained by using the least square method. The conversion coefficients are 1317.61 mN/V, 790.20 mN/V, 134.17 mN/V, 361.46 mN/V for finger 1,2, 3, 4 respectively. Similarly, the conversion coefficients between the output voltages of strain gauge glued on fingers with planar surface and the grasping forces can be calibrated as 880.28 mN/V, 700.90 mN/V, 689.04 mN/V, 3564.82 mN/V, respectively.

Experimental tests were carried out to investigate the influence of the preload force and contact distance on the admissible contact force by applying increasing contact force on the gripped hole. The contacting state of the gripped hole and fingers can be divided into three stages as shown in Fig. 7: (A) planar contact without contact force, (B) planar contact with contact force and (C) rotating or sliding. The grasping forces were collected and summarized in Fig. 8 and Fig. 9. The admissible contact force is increasing with the increment of preload fore, while it is decreasing with the increment of contact displacement. As depicted in these two pictures, the grasping force 1 and grasping force 2 increases and decreases linearly with the increasing of the contact force respectively, when the contact force is less than the admissible contact force. When the contact force exceeds the admissible contact force, the gripped hole rotates and the grasping force changes with nonlinearity. The changing principle and the amplitude of grasping force 3 and grasping force 4 are almost the same with those of grasping force 1 and grasping force 2.

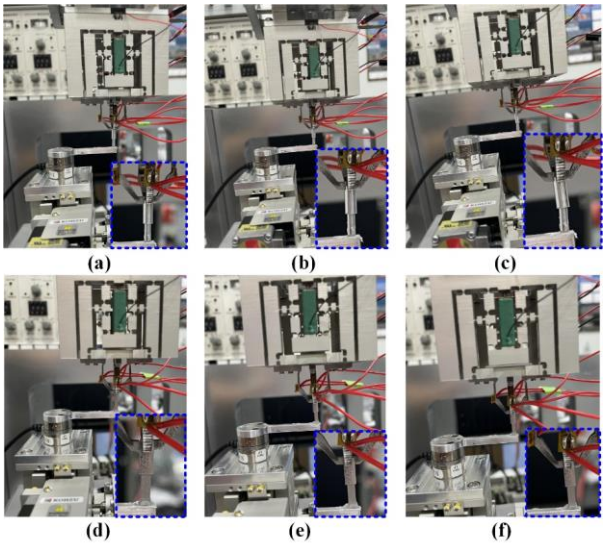

Fig. 7. The different contact states between cylindical hole and micromanipulator: (a) planar contact without contact force, (b) planar contact with contact force, (c) rotating or sliding; and the different contact states between cubicl hole and micromanipulator: (a) planar contact without contact force, (b) planar contact with contact force, (c) rotating or sliding.

When the contact distance was fixed at 4 mm and the preload force varies from 30 mN to 40 mN during the cylindrical peg-hole assembly, the admissible contact forces are 26.52 mN and 33.29 mN, respectively, as shown in Fig. 8. When the contact distance changed to 5 mm, the admissible contact forces are 22.19 mN and 30.75 mN, respectively. As shown in Fig. 9, when the contact distance was fixed at 4 mm and the preload force varies from 30 mN to 40 mN during the cuboid peg-hole assembly, the admissible contact forces are 16.71 mN and 23.44 mN, respectively. When the contact distance changed to 5 mm, the admissible contact forces are 15.2 mN and 18.83 mN, respectively. The admissible contact forces under different

condition were summarized in Table 1. It is shown that the value calculated by theoretical model and experimental tests are consistent, and the error is below 15%.

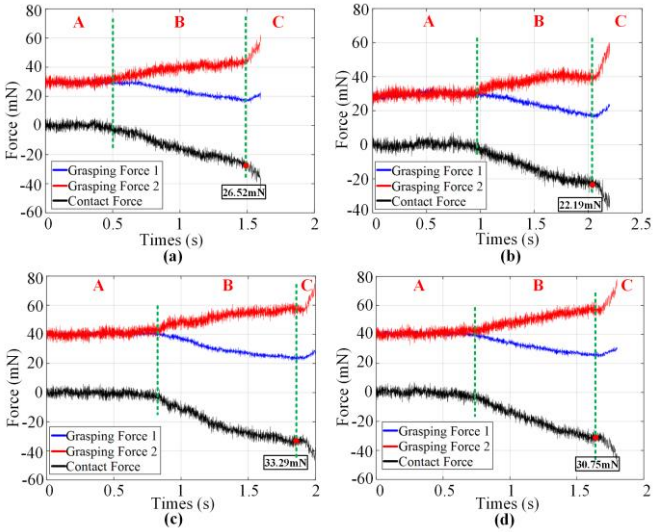

Fig. 8. The admissible contact force for cylindrical hole grasping when (a) preload force is 30 mN and contact distant is 4 mm, (b) preload force is 30 mN and contact distant is 5 mm, (c) preload force is 40 mN and contact distant is 4 mm, (d) preload force is 40 mN and contact distant is 5 mm.

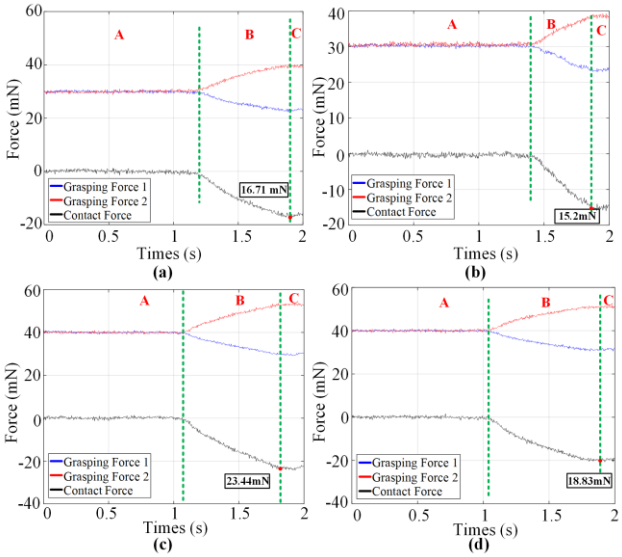

Fig. 9. The admissible contact force for cuboid hole grasping when (a) preload force is 30 mN and contact distant is 4 mm, (b) preload force is 30 mN and contact distant is 5 mm, (c) preload force is 40 mN and contact distant is 4 mm, (d) preload force is 40 mN and contact distant is 5 mm.

TABLE I

THE COMPARISON OF THEORETICAL VALUE AND EXPERIMENTAL VALUE OF ADMISSIBLE CONTACT FORCE

Object	cylinder				cube			
Preload Force (mN)	30		40		30		40	
Contact Distance (mm)	4	5	4	5	4	5	4	5
Theoretical value (mN)	28.98	23.19	38.64	30.91	18.39	14.71	24.51	19.61
Experimental value (mN)	26.52	22.19	33.29	30.75	16.71	15.2	23.44	18.83
Error	9.28%	4.31%	13.85%	0.52%	9.14%	9.14%	4.37%	3.98%

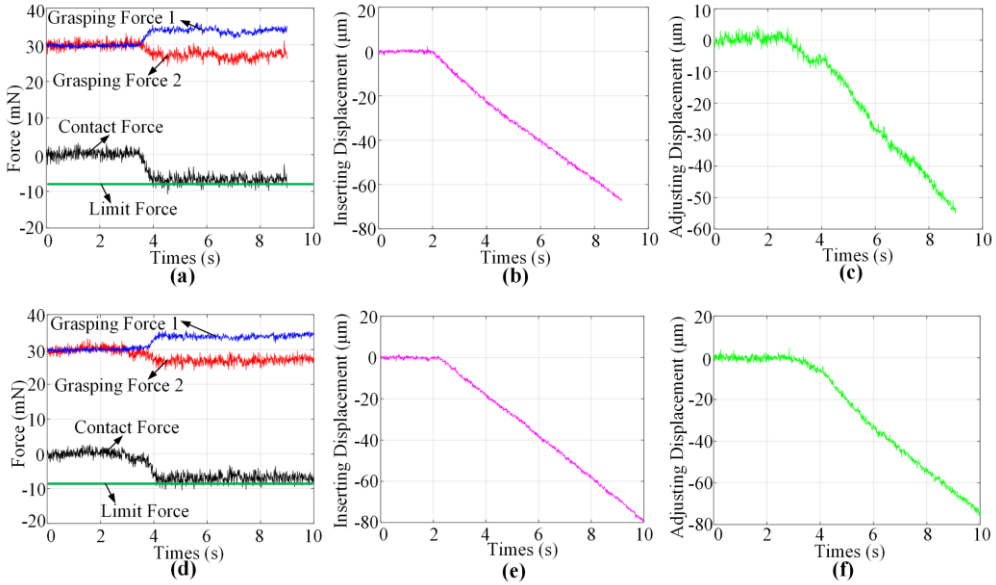

Fig.10. (a) The grasping force and contact force, (b) the inserting distance, (c) the adjusting displacement, of the cylindrical peg-hole inserting process with low contact step increment; (d) The grasping force and contact force, (e) the inserting distance, (f) the adjusting displacement, of the cuboid peg-hole inserting process with low contact step increment.

The robustness of the control strategy was investigated by carrying out a peg-in-hole simulated inserting task, during which contact perturbation were applied on the gripped hole by the precise platform continuously. It can be seen from Fig. 10, the preload grasping forces with the amplitude of 30 mN were applied on the gripped hole to pick it up steadily. According to the sensor noise and the admissible contact force measurement, the threshold 1 and threshold 2 were set as 8 mN and 15 mN. The contact force increased to the threshold 1 when the peg moves forward with a slow contacting speed of 0.25 μm/s and a step increment of 0.25 μm. Then, the controller started working and the contact force was maintained under the threshold (8 mN) instead of increasing all the time. The reason for this phenomenon is that the correcting motion with the speed of 10 μm/s and a step increment of 0.5 μm is higher than that of contacting motion. During this process, the inserting operation wasn't stopped and the manipulation was completed successfully because the contact force wasn't reached the threshold 2.

Then, a step perturbation with a contacting speed of 2.5 μm/s and step increment of 2.5 μm was applied on the gripped hole to estimate the performance of the controller. The grasping forces, the inserting displacement and the adjusting displacement were collected as shown in Fig. 11. As can be seen from Fig. 11(a) and (d), the contact force exceeded 15 mN fast because the contacting speed and the step increment is higher. The controller switched on and the insertion was stopped to keep stable grasping and to avoid damaging the micro parts during which the contact force exceeded the threshold 2 as shown in Fig. 11(b) and (e). When the contact force was corrected under 15 mN, the peg was restarted inserting into the hole and reached the desired position. As can be seen from Fig. 11(a) and (d), the contacting force can be limited below threshold 1 (8 mN) finally. The insertion with high contact force can also be achieved successfully, which verified the fine performance of the controller.

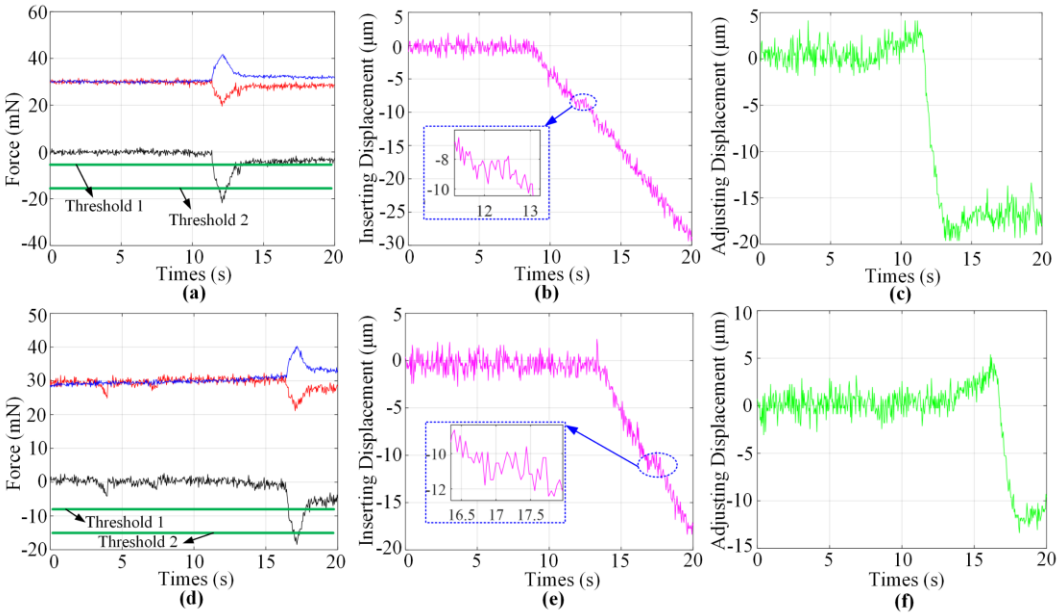

Fig.11. (a) the grasping force and contact force, (b) the inserting distance, (c) the adjusting displacement, of the cylindrical peg-hole simulated inserting process with high contact step increment; (d) The grasping force and contact force, (e) the inserting distance, (f) the adjusting displacement, of the cuboid peg-hole simulated inserting process with high contact step increment.

V. Conclusion

This paper proposes a novel contact force sensing and control method. Different from the existing methods, the force sensors integrated in the micromanipulator are used to detect the grasping force and lateral contact force, which reduces the influence of the mass of the micromanipulator on the test results. To avoid the rotating of the gripped hole, the admissible contact force is analyzed by establishing the theoretical model and is set as the reference for force threshold in the control algorithm. Experimental test is carried out to investigate the admissible contact force before the rotation of the gripped hole. The test results are consisted with the theoretical results and the error is smaller than 15%. The effectiveness of the proposed contact force sensing and control method is verified by conducting experiments of applying contact force on the gripped hole with different contacting speeds. Experimental results indicate that the inserting motion will stop when the contact force exceeds force threshold 2 (15 mN) and the contact force can be controlled to be smaller than force threshold 1 (8 mN) finally under the action of the proposed method.

References

[1] J. Cho, S. Kang and K. Kim, "Real-Time Precise Object Segmentation Using a Pixel-Wise Coarse-Fine Method with Deep Learning for Automated Manufacturing," Journal of Manufacturing Systems, vol. 62, pp. 114-123, Jan. 2022.

[2] T. Q. Xu, J. C. Zhang, M. Salehizadeh, O, Onaizah and E. Diller, "Millimeter-Scale Flexible Robots with Programmable Three-

Dimensional Magnetization and Motions," Science Robotics, vol. 4, no. 29, Apr. 2019.
[3] P. Gutruf, V. Krishnamurthi, A. Vazquez-Guardado, Z. Q. Xie et al. "Fully Implantable Optoelectronic Systems for Battery-Free, Multimodal Operation in Neuroscience Research," Nature Electronics, vol. 1, no. 12, pp. 652-660, Dec. 2018.
[4] A. N. Das, R. Murthy, D. O. Popa, and H. E. Stephanou, "A Multiscale Assembly and Packaging System for Manufacturing of Complex Micro/nano Devices," IEEE Transaction on Automation Science and Engineering, vol. 9, no. 1, pp. 160–170, Jan. 2012.
[5] M. S. Choi, Y. W. Shin, G.R. Jang, D. H. Lee, J. H. Park and J. H. Bae, "Kinesthetic Sensing for Peg-In-Hole Assembly Based on In-Hand Manipulation," IEEE Robotics and Automation Letters, vol. 6, no. 4, pp. 8418-8425, Oct. 2021.
[6] H. Park, J. Park, D. H. Lee, J. H. Park, M. H. Baeg and J. H. Bae, "Compliance-Based Robotic Peg-in-Hole Assembly Strategy Without Force Feedback," IEEE Transaction on Industrial Electronics, vol. 64, no. 8, pp. 6299-6309, Aug. 2017.
[7] J. Takahashi, T. Fukukawa and T. Fukuda, "Passive Alignment Principle for Robotic Assembly Between a Ring and a Shaft with Extremely Narrow Clearance," IEEE-ASME Transactions on Mechatronics, vol. 21, no. 1, pp. 196-204, Feb. 2016.
[8] Y. C. Tseng, K. Y. Chang, P. L. Liu, and C. C. Chang, "Applying the Purdue Pegboard to Evaluate Precision Assembly Performance," 2017 IEEE International Conference on Industrial Engineering and Engineering Management, pp: 1179-1183, Dec. 2017.
[9] Y. Taira, H. Numata and T. Barwicz, "Precision Assembly of Polymer Waveguide Components for Silicon Photonic Packaging," 2014 IEEE CPMT Symposium Japan, pp: 63-66, Nov. 2014.
[10] Y. L. Tian, Z. C. Huo, F. J. Wang, C. M. Liang, B. C. Shi and D. W. Zhang, "A Novel Friction-Actuated 2-DOF High Precision Positioning Stage with Hybrid Decoupling Structure," Mechanism and Machine Theory, vol. 167, Jan. 2022.
[11] J. H. Su, C. K. Liu and R. Li, "Robot Precision Assembly Combining with Passive and Active Compliant Motions," IEEE Transaction on Industrial Electronics, vol. 69, no. 8, pp. 8157-8167, Aug. 2022.
[12] B. C. Shi, F. J. Wang, Z. C. Huo, Y. L. Tian, X. L. Zhao and D. W. Zhang, "Design of a Rhombus-Type Stick-Slip Actuator with Two Driving Modes for Micropositioning," Mechanical Systems and Signal Processing, vol. 166, Mar. 2022.
[13] J. Zhang, D. Xu, Z. T. Zhang, and W. S. Zhang, "Position/Force Hybrid Control System for High Precision Aligning of Small Gripper to Ring Object," International Journal of Automation and Computing, vol. 10, no. 4, pp. 360-367, Aug. 2013.
[14] Y. H. Gai, J. M. Guo, D. Wu and K. Chen, "Feature-Based Compliance Control for Precise Peg-in-Hole Assembly," IEEE Transaction on Industrial Electronics, vol. 69, no. 9, pp. 9309-9319, Apr. 2022.
[15] Y. Li, Z. J. Zhang, X. Ye and S. J. Chen, "A Novel Micro-Assembly Method Based on the Mapping Between Assembly Force and Position," International Journal of Advanced Manufacturing Technology, vol. 86, no. 1-4, pp. 227-236, Sep. 2016.
[16] S. Liu, Y. F. Li and D. P. Xing, "Sensing and Control for Simultaneous Precision Peg-in-Hole Assembly of Multiple Objects," IEEE Transaction on Automation Science and Engineering, vol. 17, no. 1, pp. 310-324, Jan. 2020.
[17] D. P. Xing, F. F. Liu, S. Liu and D. Xu, "Efficient Insertion of Partially Flexible Objects in Precision Assembly," IEEE Transaction on Automation Science and Engineering, vol. 16, no. 2, pp. 706-715, Apr. 2019.
[18] Z. M. Hou, Z. H. Li, C. W. Hsu, K. G. Zhang and J. Xu, "Fuzzy Logic-Driven Variable Time-Scale Prediction-Based Reinforcement Learning for Robotic Multiple Peg-in-Hole Assembly," IEEE Transaction on Automation Science and Engineering, vol. 19, no. 1, pp. 218–229, Jan. 2022.
[19] F. J. Wang, B. C. Shi, Y. L. Tian, Z. C. Huo, X. Y. Zhao and D. W. Zhang, "Design of a Novel Dual-Axis Micromanipulator with an Asymmetric Compliant Structure," IEEE-ASME Transactions on Mechatronics, vol. 24, no. 2, pp. 656-665, Apr. 2019.
[20] T. Chen, Y. Q. Wang, Z. Yang, H. C. Liu, J. Y. Liu and L. N. Sun, "A PZT Actuated Triple-Finger Gripper for Multi-Target Micromanipulation," Micromachines, Vol. 8, no. 2, pp: 33, Feb. 2017.
[21] Y. L. Liu and Q. S. Xu, "Mechanical Design, Analysis and Testing of a Large-Range Compliant Microgripper" Mechanical Sciences, vol. 7, no. 1, pp. 119-126, Apr. 2016.
[22] L. A. Velosa-Moncada, L. A. Aguilera-Cortes, M. A. Gonzalez-Palacios, J. P. Raskin and A. L. Herrera-May, "Design of a Novel MEMS Microgripper with Rotatory Electrostatic Comb-Drive Actuators for Biomedical Applications," Sensors, vol. 18, no. 5, May. 2018.
[23] S. Saito, K. Kawamura, R. Dhelika, P. Hemthavy, K. Takahashi, W. Takarada and T. Kikutani, "Force Evaluation of Electrostatic Gripper with Arrayed Fibers Consisting of Parallel and Coaxial Electrodes," Smart Materials and Structures, vol. 28, no. 9, Sep. 2019.
[24] X. H. Huang, C. Liu and M. Wang, "An Automatic Vacuum Microgripper," 2010 8th World Congress on Intelligent Control and Automation (WCICA), pp: 5528-5532, Jul. 2010.
[25] B. Komati, K. Rabenorosoa, C. Clevy and P. Lutz, "Automated Guiding Task of a Flexible Micropart Using a Two-Sensing-Finger Microgripper," IEEE Transaction on Automation Science and Engineering, vol. 10, no. 3, pp. 515-524, Jul. 2013.
[26] F. J. Wang, B. C. Shi, Z. C. Huo, Y. L. Tian and D. W. Zhang, "Design and Control of a Spatial Micromanipulator Inspired by Deployable Structure," IEEE Transaction on Industrial Electronics, vol. 69, no. 1, pp. 971-979, Jan. 2022.

Beichao Shi received the B.Eng. degree in mechanical engineering from the School of Mechanical Engineering, Hefei University of Technology, Hefei, China, in 2016, and the M.Sc. degrees in mechanical engineering from Tianjin University, Tianjin, China, in 2019. He is currently working towards the Ph.D. degree in mechanical engineering at the School of Mechanical Engineering, Tianjin University, Tianjin, China.
His current research interests include flexure mechanism, macro/micro manipulation and control.

Fujun Wang received the B.Eng. degree in mechanical engineering from Hebei University of Technology in 2005, and the M.Sc. and Ph.D. degrees in mechanical engineering from Tianjin University, Tianjin, China, in 2007 and 2010, respectively.
In 2010, he became an Assistant Professor with the School of Mechanical Engineering, Tianjin University, where he is currently a Professor. He was a research scholar in Department of Mechanical Science and Engineering, University of Illinois at Urbana-Champaign, Urbana, USA from 2013 to 2014.
His current research interests include micro/nano manipulation and positioning, micro/nano manufacturing, dynamics and control, flexure actuator and robots.

Zhichen Huo received the B.Eng. degree in mechanical engineering from the School of Mechanical Engineering, Wuhan University of Technology, Wuhan, China, in 2014. He is currently working towards the Ph.D. degree in Mechanical Engineering at the School of Mechanical Engineering, Tianjin University, Tianjin, China.
His current research interests include flexure mechanism, dynamic and control, and micro/nano manufacturing.

Yanling Tian received the Ph.D. degree in mechanical engineering from Tianjin University, Tianjin, China, in 2005.
He is currently an Associate Professor with school of engineering, the University of Warwick, U.K., in 2006. His research interests include micro/nano manipulation, mechanical dynamics, surface metrology and characterization.
Dr. Tian was the recipient of the prestigious Alexander von Humboldt Fellowship for experienced researchers in 2010.

Ren Cong received the B.Eng. degree in mechanical engineering from the School of Mechanical Engineering, Tianjin University of Technology, Tianjin, China, in 2021. He is currently working towards the B.S. degree in mechanical engineering at the School of Mechanical Engineering, Tianjin University, Tianjin, China.

His current research interests include macro/micro manipulation robot and control

Dawei Zhang received the B.Eng. degree in mechanical engineering from Shenyang University of Technology, Shenyang, China, in 1984, and the M.Sc. and Ph.D. degrees in mechanical engineering from Tianjin University, Tianjin, China, in 1990 and 1995, respectively.

He is currently a Professor with the School of Mechanical Engineering, Tianjin University. He has been a Visiting Scholar at Hongkong University of Science and Technology, Clear Water Bay, Hong Kong; the University of Warwick, Coventry, U.K.; and Tokyo Institute of Technology, Tokyo, Japan. His current research interests include dynamics and machine tools.